White Rose Research Online

eprints@whiterose.ac.uk
https://eprints.whiterose.ac.uk
Universities of Leeds, Sheffield and York

Deposited via The University of Sheffield.

White Rose Research Online URL for this paper:
https://eprints.whiterose.ac.uk/id/eprint/136606/

Version: Accepted Version

Article:
Barr, A.D., Clarke, S. and Petkovski, M. (2019) High-pressure compressibility and shear strength data for soils. Canadian Geotechnical Journal, 56 (7). pp. 1042-1048. ISSN: 0008-3674

https://doi.org/10.1139/cgj-2018-0235

© 2018 The Authors. This is an author-produced version of a paper subsequently published in Canadian Geotechnical Journal. Uploaded in accordance with the publisher's self-archiving policy.

Reuse
Items deposited in White Rose Research Online are protected by copyright, with all rights reserved unless indicated otherwise. They may be downloaded and/or printed for private study, or other acts as permitted by national copyright laws. The publisher or other rights holders may allow further reproduction and re-use of the full text version. This is indicated by the licence information on the White Rose Research Online record for the item.

Takedown
If you consider content in White Rose Research Online to be in breach of UK law, please notify us by emailing eprints@whiterose.ac.uk including the URL of the record and the reason for the withdrawal request.

UNIVERSITY OF LEEDS
University of Sheffield
UNIVERSITY of York

High-pressure compressibility and shear strength data for soils

A. D. Barr[1*], S. D. Clarke[1], M. Petkovski[1]

[1] Department of Civil and Structural Engineering, The University of Sheffield, Sir Frederick Mappin Building, Mappin Street, Sheffield, S1 3JD, UK

* Corresponding author (a.barr@sheffield.ac.uk)

Abstract

Soil behaviour is often an important consideration in the design of protective systems for blast and impact threats, as the properties of a soil can greatly affect the impulse generated from buried explosive devices, or the ability of a soil-filled structure to resist ballistic threats. Numerical modelling of these events often relies on extrapolation from low-pressure experiments. In order to develop soil models which remain accurate at very high pressures there is a need for data on soil behaviour under these extreme conditions. This paper demonstrates the use of a high-pressure multi-axial test apparatus to provide compressibility and shear strength data for four dry sandy soils. One-dimensional compression experiments were performed to axial stresses of 800 MPa, where the effects of particle size distribution were observed with respect to compressibility and bulk unloading modulus. Each soil followed a bi-linear NCL: more uniform soils initially had higher compression indices, but all four NCLs began to converge at void ratios below $e \approx 0.3$. The failure surface of a sand was characterised to $p' > 400$ MPa using reduced triaxial compression experiments, removing the need to rely on extrapolation from low-pressure data.

Keywords: high pressure; compressibility; shear strength; sand; blast; impact

Introduction

Soil-filled wire and geotextile gabions are commonly used to construct defensive infrastructure in military bases, as the attenuating properties of soils can help protect against blast and fragmentation effects (Warren et al. 2013). Soils also significantly affect the impulse generated by buried mines and improvised explosive devices (IEDs), with implications for the structural response of protective systems and decision making in civilian demining operations (Clarke et al. 2017). In order to adapt to new threats and develop robust constitutive models, the designers of protective systems require high-pressure data on the behaviour of soils over a wide range of ground conditions, particularly for common sandy soils.

The pressures produced in blast and impact events are much higher than those in most civil engineering applications: the peak overpressure around a buried explosion is typically hundreds of megapascals. One-dimensional compression of sands in high-pressure oedometer experiments has shown that large strains and extensive particle crushing occur at these stresses, and that soil stiffness and crushing are dependent on particle size distribution and mineralogy (Fukumoto 1992, McDowell 2002, Chuhan et al. 2003). Hagerty et al. (1993) tested quartz sand, slag and glass bead specimens at stresses up to $689\,\mathrm{MPa}$ and found that particle crushing increased with increased angularity and increased median particle size, and began at lower stresses for angular and loose specimens. Yamamuro et al. (1996) investigated the effect of mineralogy using tests on quartz and gypsum sands and an intermediate hardness sand to $850\,\mathrm{MPa}$. As well as being more compressible, the softer soils showed less sensitivity to initial density, as differences in initial void ratio disappeared at lower stresses than in the quartz sand. The effects of particle size and particle size distribution in quasi-static testing have also been replicated in the high-strain-rate regime: well graded soils tend to be less compressible than uniform soils and experience less particle breakage (Farr 1990, Huang et al. 2013), and finer soils are less compressible and experience less particle breakage than coarse soils (Luo et al. 2014). High strain rates ($10^2\,\mathrm{s}^{-1}$ to $10^6\,\mathrm{s}^{-1}$) have been

shown not to have a significant effect on the compressibility of quartz sands once inertial effects are accounted for (Song et al. 2009, Bragov et al. 2008, Barr et al. 2016*b*), and so numerical models can be calibrated reliably using quasi-static data from high-pressure experiments.

Triaxial testing at the pressures experienced in blast and impact events is much less developed, with many numerical models relying on shear behaviour extrapolated from standard laboratory tests. Investigations at lower stresses have shown that confining pressure has a significant effect on the mechanisms which contribute to shearing resistance, as increasing confinement leads to a reduction in dilation and interlocking (Guo and Su 2007) and an increase in the contribution of particle breakage and rearrangement (Hall and Gordon 1964, Marachi 1969). At high pressures ($\sigma_3 = 310\,\mathrm{MPa}$), Murphy (1971) used a triaxial cell to show that an increase in the mineral hardness of a soil results in an increase in shear strength and a reduction in compressibility. Martin and Cazacu (2013) also used a triaxial cell to characterise the strength and elastic properties of a quartz sand at high pressures ($\sigma_3 \leq 300\,\mathrm{MPa}$), and successfully defined a linear failure surface and stress-dependent elastic moduli. Both compression and dilation were observed during deviatoric loading in these experiments. Recent triaxial testing approaches (Martin et al. 2013, Barr et al. 2016*a*) have begun to explore the shear response of soils at very high strain rates: further comparison with high-pressure quasi-static data is required to investigate whether existing models of shear behaviour hold under this extreme loading.

This paper demonstrates the use of a high-pressure multi-axial test apparatus to characterise the quasi-static compressibility and failure surface of quartz sands to pressures of $800\,\mathrm{MPa}$ and $400\,\mathrm{MPa}$, respectively. The multi-axial nature of the apparatus means that many other stress paths are possible, including cyclic experiments, stress probes and tests at different Lode angles. The current experiments provide data which can be used to calibrate existing material models for sands, and which can support research into the high-strain-rate shear behaviour of soils.

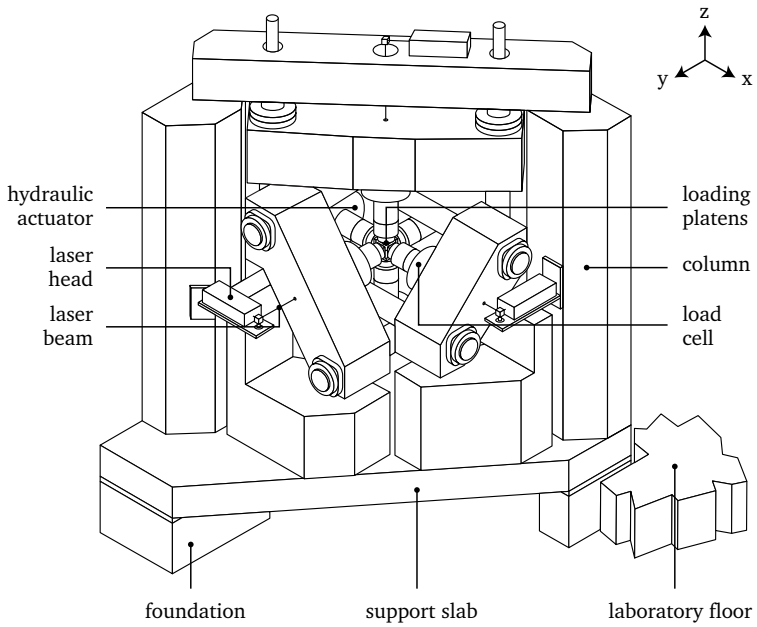

Figure 1: The mac^{2T} test apparatus.

High-pressure multi-axial apparatus

The high-pressure one-dimensional compression and triaxial tests in this paper were carried using mac^{2T} (pronounced *MASS-et*), a test apparatus for Multi-Axial Compression of Concrete at Elevated Temperatures (Petkovski et al. 2006). The mac^{2T} test apparatus, shown in Figure 1, allows specimens to be tested in true multi-axial compression ($\sigma_x \neq \sigma_y \neq \sigma_z$), with independent control of loads or displacements in the x, y and z directions. In each axis the load is applied by a $4\,\mathrm{MN}$ hydraulic actuator installed in an independent loading frame.

Each loading frame (Figure 2) contains a load cell which is rated at $4\,\mathrm{MN}$ and operates to an accuracy of $\pm 4\,\mathrm{kN}$. Loads are transmitted from the actuator to the specimen, and from the specimen to the load cell, by $200\,\mathrm{mm}$ diameter steel rams, which each terminate in a $95 \times 95\,\mathrm{mm}$ steel loading platen, initially designed for $100 \times 100\,\mathrm{mm}$ concrete cubes.

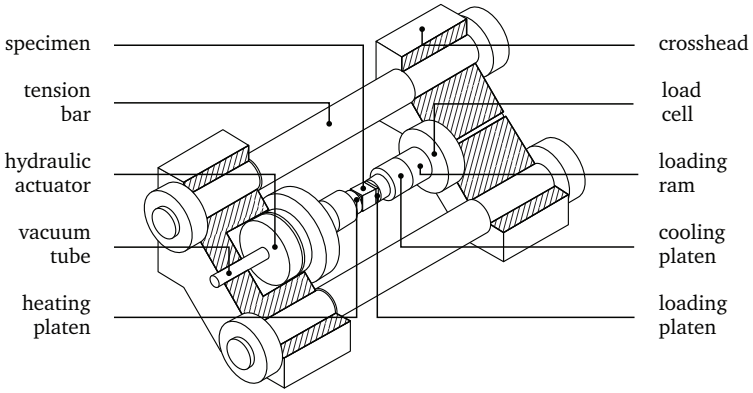

Figure 2: The mac^{2T} x-axis loading frame. Hatching indicates a section cut.

The displacement of each specimen face is measured to an accuracy of $\pm 1\,\mu\mathrm{m}$ by a laser interferometer, which operates along an evacuated stainless steel tube inside the loading ram. Data acquisition and control of the loads, displacements and temperatures in the apparatus are managed by a purpose-built LabVIEW program, which is described in more detail by Petkovski et al. (2006).

Sand test box

In tests on concrete the specimen cube is $5\,\mathrm{mm}$ larger than the loading platens, and so experiments can be carried out without the platens ever touching. To enable the testing of highly compressible, cohesionless soils, a special loading box was fabricated to contain the sand during testing. The test box is made up of six case-hardened steel blocks which can be arranged to form an interior cube. The dimensions and assembly of the box are depicted in Figure 3, which also shows the axis convention used throughout this work. The bolts are countersunk in oversized holes: this allows the interior dimensions of the box to be fixed during specimen preparation, while allowing the relative displacement of all six faces during testing.

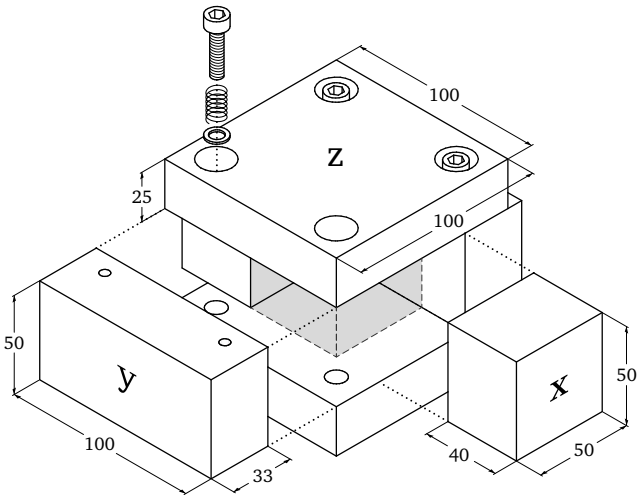

Figure 3: Exploded view of sand loading box, indicating axes convention. Dimensions in mm. Specimen location is shaded.

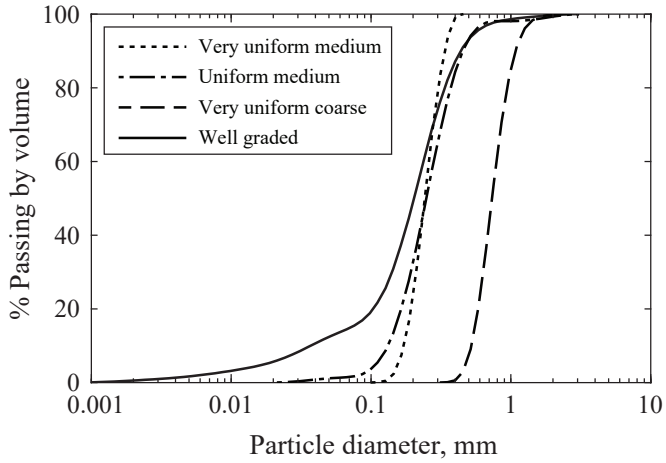

Figure 4: Particle size distributions of the four quartz sands tested.

Soil properties

This paper provides experimental data for four sandy soils, which are commonly encountered in buried blast events and are often used as fill material in protective gabion structures. All four soils are quartz sands with a variety of particle size distributions, as shown in Figure 4 and Table 1. The well-graded and uniform medium sands also contain 13% and 2% silt by mass, respectively. The mineralogy of the specimens was assessed using x-ray diffraction and confirmed that all four soils are predominantly formed of quartz. The well-graded and uniform medium sands also contain minor quantities of microcline, and uniform medium sand contains minor quantities of augite. All experiments were performed on dry soil prepared at a density of $1.5\,\mathrm{Mg\,m^{-3}}$ ($e = 0.71$), and initial specimen dimensions were $50\,\mathrm{mm} \times 50\,\mathrm{mm} \times 50\,\mathrm{mm}$ unless otherwise noted.

One-dimensional compression

In a one-dimensional compression experiment the specimen is deformed along one axis, while deformations in the other two directions are kept at zero. To achieve this in mac^{2T}, the load was applied in the x-axis under load control, while the other two axes were kept under displacement control, recording the stress required to maintain zero deformation.

Method

Figure 5 shows an example of a one-dimensional compression experiment on uniform medium sand. At the beginning of the experiment the specimen was placed into mac^{2T} and the loading platens in each axis were brought into contact with the sand test box. A load of $7\,\mathrm{kN}$ ($2.8\,\mathrm{MPa}$) was applied to each face of the test box to initialise the position of the interferometers (Point 1). The specimen was then loaded at a relatively low rate of $20\,\mathrm{MPa\,min^{-1}}$ to $\sigma_x = 40\,\mathrm{MPa}$ (Point 2), with a peak strain rate of approximately $10^{-3}\,\mathrm{s^{-1}}$. The y- and z-axis loading platens

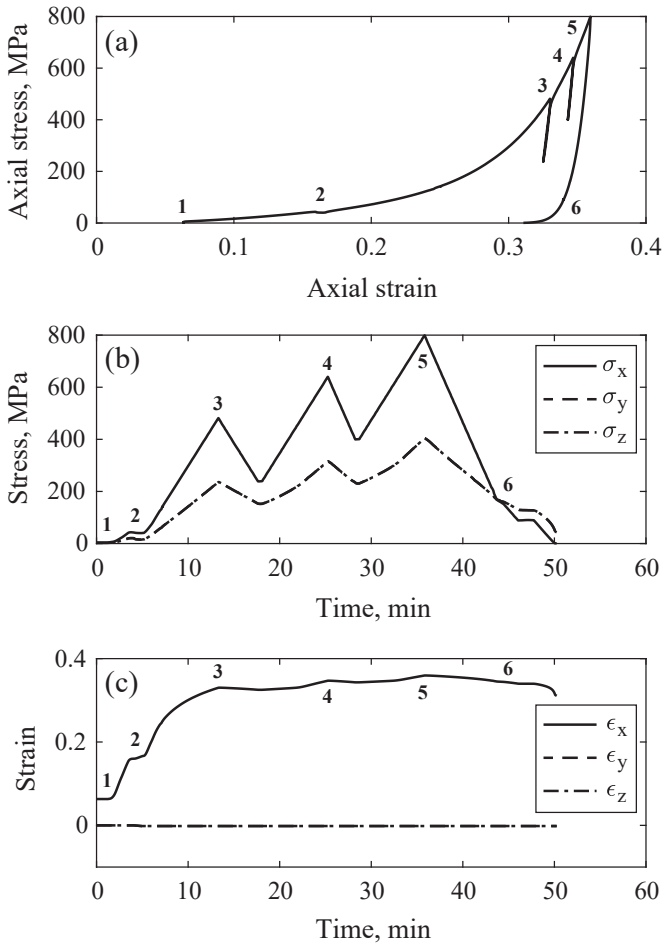

Figure 5: High-pressure one-dimensional compression experiment on dry uniform medium sand: a) Axial stress–axial strain, b) stress–time and c) strain–time. Stresses and strains in the y and z axes are coincident.

were backed off by $0.1\,\mathrm{mm}$ at this point to ensure that friction between the sand test box blocks did not significantly contribute to the stiffness of the soil specimen at higher stresses. Loading to the peak axial stress of $800\,\mathrm{MPa}$ was carried out in three cycles (Points 2–5), at a constant loading rate of $60\,\mathrm{MPa\,min^{-1}}$: these load cycles were performed in order to determine the hysteretic behaviour of the soil, and to provide data for calculating the unloading stiffness at different stress levels. The specimen was unloaded by reducing the axial stress until it was equal to the two minor stresses (Point 6), and then all stresses were reduced to zero, so that the sample remained intact for further study.

This method was used to test three specimens of each soil, with repeatable results (Figure 6a). The sensitivity of the stress-strain behaviour to variations in quasi-static loading rates was also investigated in an experiment where the axial stress was applied at $250\,\mathrm{MPa\,min^{-1}}$: the stress-strain curve was identical to those in the tests where the specimen was loaded at $60\,\mathrm{MPa\,min^{-1}}$, as shown in Figure 6a.

Results

Following one-dimensional compression to $800\,\mathrm{MPa}$, all four soils could be removed from the test box as a block of solid material (Figure 7). These blocks remained intact under significant unconfined loading: a block of medium sand tested in a state of uniaxial stress along the original loading axis failed at a stress of $3.2\,\mathrm{MPa}$. The grey markings on the surface of the sand block are evidence of friction with the interior of the steel test box; however, an experiment performed with a shorter $30\,\mathrm{mm}$ specimen did not show a significant effect of friction on the recorded soil behaviour (Figure 6a).

Mean results for the four soils are shown in Figure 6b. At $800\,\mathrm{MPa}$ the soils achieved void ratios between 0.08 and 0.15, equating to dry densities between $2.31\,\mathrm{Mg\,m^{-3}}$ and $2.43\,\mathrm{Mg\,m^{-3}}$. In each soil convergence on a unique normal compression line (NCL_1) was followed by further stiffening at low void ratios (NCL_2),

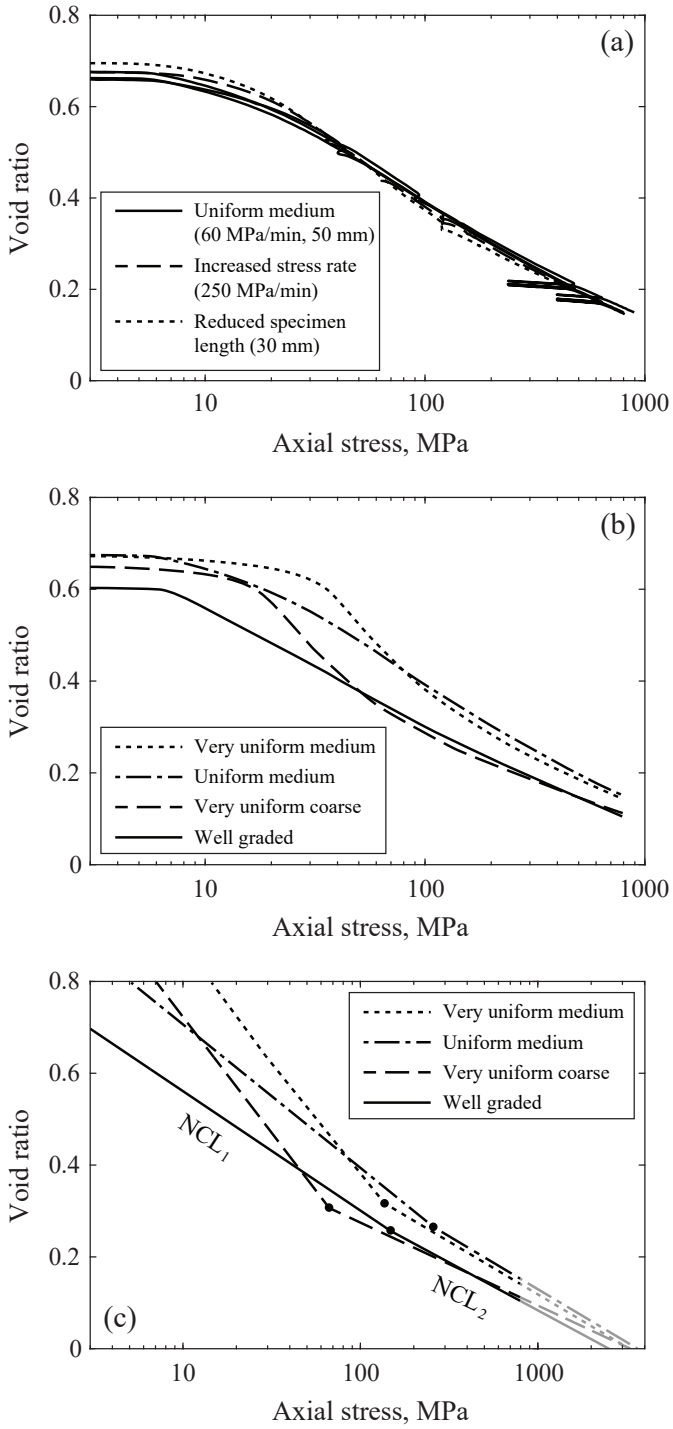

Figure 6: a) Repeatability of one-dimensional compression experiments and the effect of stress rate and specimen length, b) the effect of particle size distribution on compressibility (mean results), and c) idealised bi-linear NCLs with extrapolation to $e = 0$ (grey lines).

Figure 7: Dry uniform medium sand after loading to 800 MPa under one-dimensional compression.

resulting in the approximately bi-linear behaviour idealised in Figure 6c:

$$e = \begin{cases} e_{0,1} - C_{c,1} \log_{10} \sigma_x & e \geq e_{\text{int}} \\ e_{0,2} - C_{c,2} \log_{10} \sigma_x & e < e_{\text{int}} \end{cases} \tag{1}$$

where e_0 is the void ratio at 1 MPa, C_c is the compression index and e_{int} is the void ratio at the intersect between NCL_1 and NCL_2. The values of these parameters are provided for each soil in Table 2. The trend at high pressures is similar to that observed by Hagerty et al. (1993), who related the increased stiffness to decreasing particle breakage caused by an increasing coordination number.

As would be observed in low-pressure oedometer tests, more uniform sands moved onto the initial NCL at higher stresses (well graded: 6 MPa, uniform medium: 20 MPa, very uniform medium: 30 MPa), and the slope of the NCL was steeper in the more uniform soils (well-graded $C_{c,1} = 0.26$, uniform medium $C_{c,1} = 0.30$, very uniform medium $C_{c,1} = 0.47$). The very uniform medium sand moved onto the NCL at a higher stress (30 MPa) than the very uniform coarse sand (15 MPa): while they had identical coefficients of uniformity ($C_u = 1.5$) there is an increased probability of breakage in larger particles (McDowell et al. 1996). The behaviour of the soils converges at low void ratios, which may indicate that the soils have developed a similar PSD through particle breakage: extrapolation of the data in

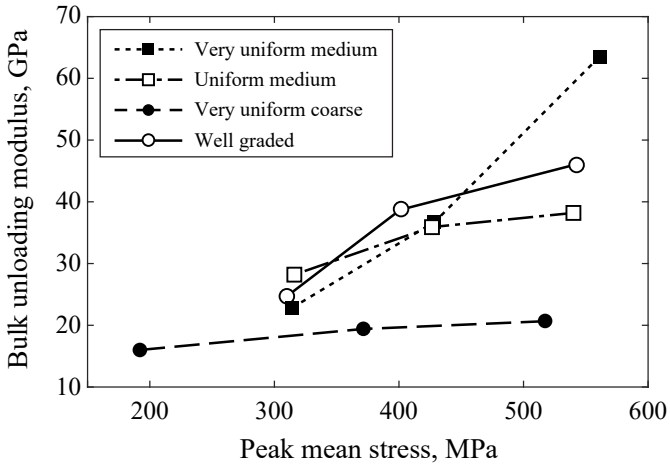

Figure 8: Variation of bulk unloading modulus with peak mean stress. Mean values shown.

Figure 6c indicates that a void ratio of zero would be achieved at approximately 3 GPa.

The unloading bulk modulus of all four soils increased as the peak stress increased, as shown in Figure 8. The well-rounded coarse sand, which was the most compressible of the soils in NCL_1, also had a significantly lower unloading modulus than the three finer, more angular soils. It is not clear how the difference in particle size distribution and particle shape have each contributed to the particle locking and packing structure in the current experiments: further experiments using μCT could be used to analyse these effects.

Reduced triaxial compression

The failure surface of the uniform medium sand was obtained at high pressures by using mac^{2T} to perform reduced triaxial compression (RTC) experiments. RTC differs from conventional triaxial compression (CTC) experiments in that deviatoric stresses are applied by reducing the cell pressure under a constant axial stress, rather than increasing axial stress under a constant cell pressure. Both CTC and

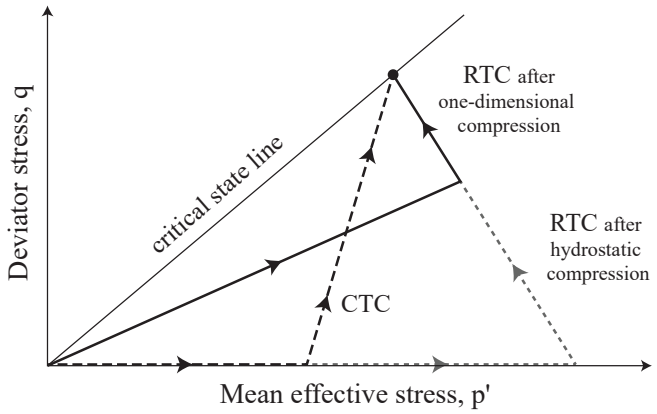

Figure 9: Stress paths in CTC and RTC tests with the same CSL intersect. The RTC experiments in this paper begin loading under one-dimensional compression (solid line) rather than hydrostatic compression (fine dashed line).

RTC experiments typically begin with hydrostatic compression, but true hydrostatic pressure cannot be applied in mac^{2T} over large displacements using the current test box design, as this would lead to contact between the loading platens. Instead, initial compaction of the sand in these RTC tests was achieved in one-dimensional compression, as shown by the stress paths in Figure 9.

Method

An example of an RTC experiment on uniform medium sand is shown in Figure 10. As before, once the sand specimen was loaded into mac^{2T} each of the axes were loaded to $7\,\mathrm{kN}$ (Point 1). The y- and z-axes were then switched to displacement control with a displacement rate of zero and, with the x-axis in load control, the specimen was loaded to $\sigma_x = 120\,\mathrm{MPa}$ in one-dimensional compression (Point 2). At this point the x- and y-axis platens were backed off by $0.1\,\mathrm{mm}$ to ensure that friction between the sand test box blocks did not contribute to the stiffness of the soil specimen. Loading then continued in one-dimensional compression to the peak mean stress, p'_0 (Point 3) – peak mean stresses of $325\,\mathrm{MPa}$, $445\,\mathrm{MPa}$ and $555\,\mathrm{MPa}$ were used in the current test series. To begin the deviatoric (RTC) portion of the

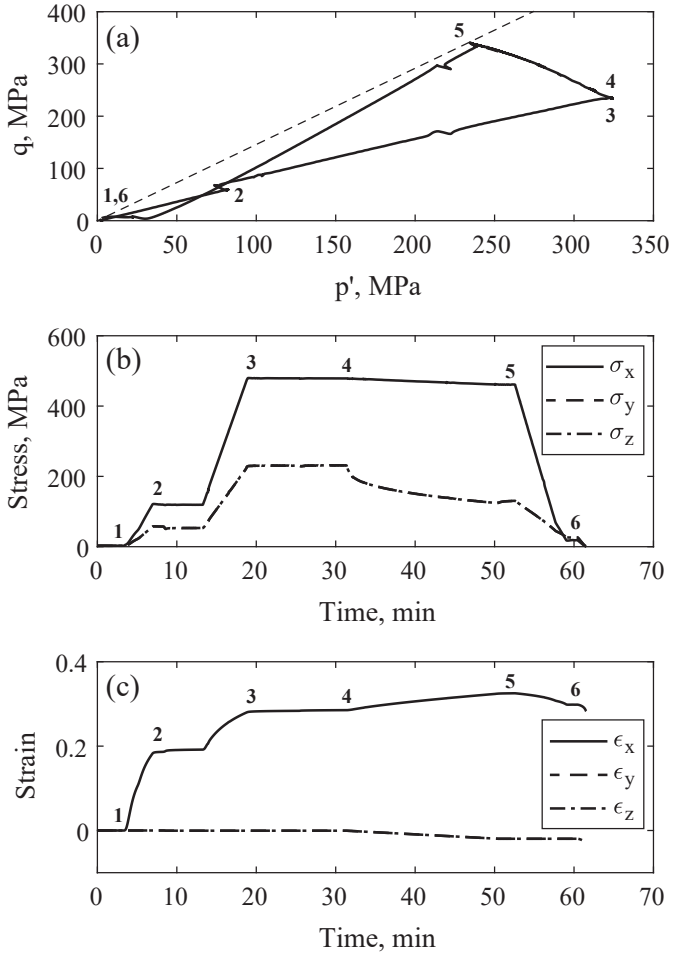

Figure 10: High-pressure reduced triaxial compression (RTC) experiment on dry uniform medium sand: a) $q - p'$ behaviour, b) stress–time and c) strain–time. Stresses and strains in the y and z axes are coincident.

experiment, the load in the x-axis was fixed by setting the loading rate to zero. The y- and z-axes were then set to a negative displacement rate, decreasing the lateral stresses, and causing the stress path to turn towards the failure surface (Point 4). A small decrease in axial stress occurred during shearing due to the increasing cross-sectional area of the x-axis. To unload the specimen, displacement of the y- and z-axes was halted (Point 5), σ_x was reduced to around $20\,\mathrm{MPa}$, and then all three axes were unloaded together (Point 6).

Results

As these are the first experiments of their kind in the literature, the high-pressure shear behaviour of the sand was not known before testing, and there was a risk that a sudden failure of the specimen would lead to a loss of control of the actuators and damage the mac$^{2\mathrm{T}}$ apparatus. To reduce this risk, lateral displacements in the current experiments were limited to $1\,\mathrm{mm}$ and, as a result, the specimens did not quite reach a critical state. However, least-squares fits to the data in Figures 11a and 11b show that each specimen was within $4\,\mathrm{MPa}$ of its ultimate strength, and so the small associated error was easily accounted for. These extrapolations also predict that the largest lateral displacement required would be approximately $1.6\,\mathrm{mm}$ (for $p'_0 = 555\,\mathrm{MPa}$), and so shearing to a critical state should be achievable in future experiments.

Figure 11c shows the results of the three RTC tests on dry uniform medium sand, which can be used to define a linear failure surface for the sand to pressures of over $400\,\mathrm{MPa}$. As the sand is cohesionless, the surface passes through the origin with a slope, M, of 1.47, equivalent to an angle of shearing resistance of $\phi'_{\mathrm{crit}} = 36.6°$. CTC experiments to similar pressures have carried out by Martin and Cazacu (2013) on a quartz sand with a similar PSD to the uniform medium sand in this paper, and these experiments also produced a linear failure surface, with an angle of shearing resistance of $\phi'_{\mathrm{crit}} = 32.3°$. There is therefore confidence that the RTC method developed in this paper can be used to characterise the shear

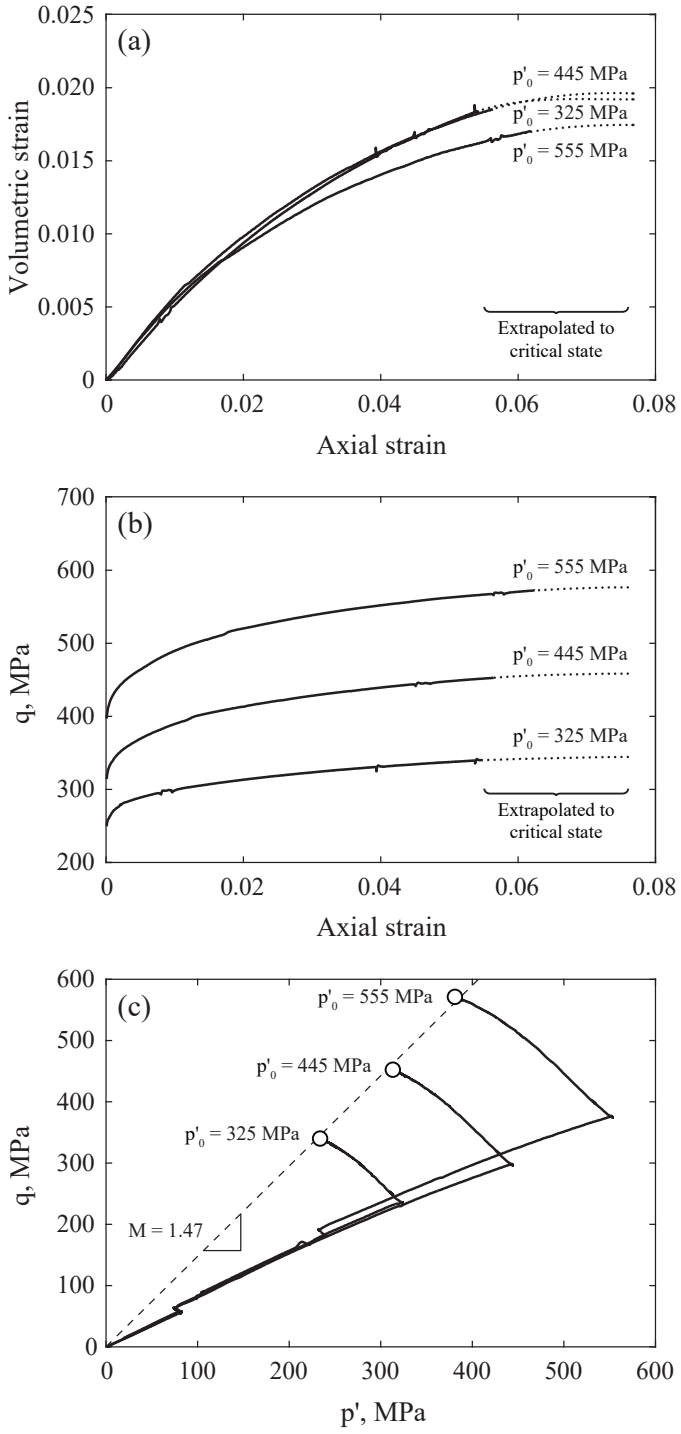

Figure 11: RTC experiments on uniform medium sand, a) $\epsilon_v - \epsilon_x$ behaviour during deviatoric loading, b) $q - \epsilon_x$ behaviour during deviatoric loading, c) $q - p'$ behaviour, with critical state line. Unloading omitted for clarity.

behaviour of soils at high pressures and, as mac^{2T} permits independent control of all three axes, there is the potential to explore more complex stress paths not possible with triaxial cell approaches.

Summary

This paper demonstrated the use of a multi-axial test apparatus to characterise soils at the high pressures encountered in blast and impact events. One-dimensional compression experiments on four sandy soils were carried out to $800\,\mathrm{MPa}$, enabling bi-linear normal compression lines to be characterised. The coarse and well-graded soils were more initially more compressible than the finer, more uniform soils, and bulk unloading moduli were shown to increase with the peak mean stress, particularly in the finer soils.

Reduced triaxial compression (RTC) experiments were used to investigate the failure surface of uniform medium sand to $p' > 400\,\mathrm{MPa}$, removing the need to rely on extrapolations from low-pressure data. Further experiments of this type will be particularly important for soils which do not exhibit a linear failure surface at high pressures, and will enable soil models to be calibrated for the simulation of blast and impact events. They will also provide valuable high-pressure quasi-static data for investigations into the high-strain-rate shear behaviour of soils.

Acknowledgements

The authors would like to thank Stephen Kerr at Dstl for his support in this work, which forms part of the Dstl-sponsored and QinetiQ-led Force Protection Engineering research programme.

References

Barr, A. D. et al. 2016*a*. Design of a split Hopkinson pressure bar with partial lateral confinement. Measurement Science and Technology, **27**(12): 1–8.

Barr, A. D. et al. 2016*b*. Effects of strain rate and moisture content on the behaviour of sand under one-dimensional compression. Experimental Mechanics, **56**(9): 1625–1639.

Bragov, A. M. et al. 2008. Determination of physicomechanical properties of soft soils from medium to high strain rates. International Journal of Impact Engineering, **35**: 967–976.

Chuhan, F. A. et al. 2003. Experimental compression of loose sands: relevance to porosity reduction during burial in sedimentary basins. Canadian Geotechnical Journal, **40**(5): 995–1011.

Clarke, S. D. et al. 2017. Predicting the role of geotechnical parameters on the output from shallow buried explosives. International Journal of Impact Engineering, **102**: 117–128.

Farr, J. V. 1990. One-dimensional loading-rate effects. Journal of Geotechnical Engineering, **116**(1): 119–135.

Fukumoto, T. 1992. Particle breakage characteristics of granular soils. Soils and Foundations, **32**(1): 26–40.

Guo, P. and Su, X. 2007. Shear strength, interparticle locking, and dilatancy of granular materials. Canadian Geotechnical Journal, **44**(5): 579–591.

Hagerty, M. M. et al. 1993. One-dimensional high-pressure compression of granular material. Journal of Geotechnical Engineering, **119**(1): 1–18.

Hall, E. and Gordon, B. 1964. Triaxial Testing with Large-Scale High Pressure Equipment. ASTM International.

Huang, J., Xu, S. and Hu, S. 2013. Effects of grain size and gradation on the dynamic responses of quartz sands. International Journal of Impact Engineering, **59**: 1–10.

Luo, H., Cooper, W. and Lu, H. 2014. Effects of particle size and moisture on the compressive behavior of dense Eglin sand under confinement at high strain rates. International Journal of Impact Engineering, **65**: 40–55.

Marachi, N. 1969. Strength and deformation characteristics of rockfill materials. PhD thesis.

Martin, B. and Cazacu, O. 2013. Experimental and theoretical investigation of the highpressure, undrained response of a cohesionless sand. International Journal for Numerical and Analytical Methods in Geomechanics, **37**(14): 2321–2347.

Martin, B. et al. 2013. Undrained high-pressure and high strain-rate response of dry sand under triaxial loading. International Journal of Impact Engineering, **54**: 51–63.

McDowell, G. 2002. On the yielding and plastic compression of sand. Soils and foundations, **42**(1): 139–145.

McDowell, G. et al. 1996. The fractal crushing of granular materials. Journal of the Mechanics and Physics of Solids, **44**(12): 2079–2102.

Murphy, D. J. 1971. High pressure experiments on soil and rock. *in* '13th Sympoium on Rock Mechanics'.

Petkovski, M. et al. 2006. Apparatus for testing concrete under multiaxial compression at elevated temperature (mac2t). Experimental Mechanics, **46**: 387–398.

Song, B. et al. 2009. Impact compressive response of dry sand. Mechanics of Materials, **41**: 777–785.

Warren, J. et al. 2013. Briefing: UK Ministry of Defence Force Protection Engineering Programme. Proceedings of the ICE - Engineering and Computational Mechanics, **166**(3): 119–123.

Yamamuro, J. A. et al. 1996. One-dimensional compression of sands at high pressures. Journal of Geotechnical Engineering, **122**(2): 147–154.

List of symbols

C_c	compressibility index
C_u	coefficient of uniformity
D_{10}	10th percentile particle size
D_{50}	50th percentile particle size
D_{60}	60th percentile particle size
e	void ratio
G_s	specific gravity
p'	mean effective stress
p'_0	maximum mean effective stress prior to deviatoric loading
q	deviatoric stress
ϵ	strain, where a subscript indicates the axis
σ	stress, where a subscript indicates the axis
ϕ'_{crit}	critical angle of shearing resistance

Tables

Table 1: Properties of the quartz sands tested. Angularity: well-rounded (WR), sub-rounded (SR) and sub-angular (SA).

Soil description (EN ISO 14688–1:2018)	D_{10} (μm)	D_{50} (μm)	D_{60} (μm)	C_u	G_s	Angularity
Very uniform coarse SAND	520	740	790	1.5	2.65	WR–SR
Very uniform medium SAND	170	230	250	1.5	2.65	SR–SA
Uniform medium SAND	130	250	280	2.2	2.65	SR–SA
Well graded silty SAND	40	200	240	6.0	2.65	SR–SA

Table 2: Compression indices for four quartz sands. Values of e_0 are taken at $1\,\mathrm{MPa}$, the subscripts 1 and 2 relate to NCL_1 and NCL_2, and e_{int} is the void ratio at the intersect of NCL_1 and NCL_2.

Soil description	$e_{0,1}$	$C_{c,1}$	$e_{0,2}$	$C_{c,2}$	e_{int}
Very uniform coarse SAND	1.22	0.50	0.66	0.19	0.31
Very uniform medium SAND	1.31	0.47	0.81	0.23	0.32
Uniform medium SAND	0.99	0.30	0.85	0.24	0.27
Well graded silty SAND	0.82	0.26	0.74	0.22	0.26

List of figure captions

- Figure 1: The mac^{2T} test apparatus.
- Figure 2: The mac^{2T} x-axis loading frame. Hatching indicates a section cut.
- Figure 3: Exploded view of sand loading box, indicating axes convention. Dimensions in mm. Specimen location is shaded.
- Figure 4: Particle size distributions of the four quartz sands tested.
- Figure 5: High-pressure one-dimensional compression experiment on dry uniform medium sand: a) Axial stress–axial strain, b) stress–time and c) strain–time. Stresses and strains in the y and z axes are coincident.
- Figure 6: a) Repeatability of mac^{2T} one-dimensional compression experiments and the effect of stress rate and specimen length, b) the effect of particle size distribution on compressibility (mean results), and c) idealised bi-linear NCLs with extrapolation to $e = 0$ (grey lines).
- Figure 7: Dry uniform medium sand after loading to 800 MPa under one-dimensional compression.
- Figure 8: Variation of bulk unloading modulus with peak mean stress. Mean values shown.
- Figure 9: Stress paths in CTC and RTC tests with the same CSL intersect. The RTC experiments in this paper begin loading under one-dimensional compression (solid line) rather than hydrostatic compression (fine dashed line).
- Figure 10: High-pressure reduced triaxial compression (RTC) experiment on dry uniform medium sand: a) $q - p'$ behaviour, b) stress–time and c) strain–time. Stresses and strains in the y and z axes are coincident.

- Figure 11: RTC experiments on uniform medium sand, a) $\epsilon_v - \epsilon_x$ behaviour during deviatoric loading, b) $q - \epsilon_x$ behaviour during deviatoric loading, c) $q - p'$ behaviour, with critical state line. Unloading omitted for clarity.